Digestive Diseases and Sciences (2023) 68:1351–1363
https://doi.org/10.1007/s10620-022-07671-w

ORIGINAL ARTICLE

NEDD8-Activating Enzyme Inhibitor MLN4924 Inhibits Both the Tumor Stroma and Angiogenesis in Pancreatic Cancer via Gli1 and REDD1

Weilin Mao[1] · Lei Zhang[1] · Yefei Rong[1] · Tiantao Kuang[1] · Dansong Wang[1] · Xuefeng Xu[1] · Wenhui Lou[1] · Jianang Li[1]

Received: 23 April 2022 / Accepted: 12 August 2022 / Published online: 13 September 2022

Abstract

Purpose Pancreatic cancer is characterized by a dense desmoplasia stroma, which hinders efficient drug delivery and plays a critical role in tumor progression and metastasis. MLN4924 is a first-in-class NEDD8-activating enzyme inhibitor that exhibits anti-tumor activities toward pancreatic cancer, and given the comprehensive effects that MLN4924 could have, we ask what impact MLN4924 would have on the stroma of pancreatic cancer and its underlying mechanisms.

Methods Primary pancreatic stellate cells (PSCs) and human HMEC-1 cells were treated with MLN4924 in vitro. The proliferation and extracellular matrix protein levels of PSCs were tested, and their relationship with transcription factor Gli1 in PSCs was investigated. The angiogenic phenotypes of HMEC-1 cells were evaluated using capillary-like tube formation assay, and their relationship with REDD1 in HMEC-1 cells was investigated.

Results In this study, we found that MLN4924 inhibited the proliferation of pancreatic stellate cells and their secretion of collagen and CXCL-1, and the collagen secretion inhibiting effect of MLN4924 was related with transcription factor Gli1. MLN4924 inhibited multiple angiogenic phenotypes of HMEC-1 cells, and mTOR agonist partially relieved the inhibition of MLN4924 on HEMCs. MLN4924 increased the expression of REDD1 and REDD1 knockdown promoted the angiogenic phenotypes of HMEC-1 cells.

Conclusions Our study suggests that MLN4924 inhibits both the tumor stroma and angiogenesis in pancreatic cancer, and the inhibition effect is related with Gli1 in pancreatic stellate cells and REDD1 in vascular endothelial cells, respectively.

Keywords Pancreatic neoplasms · Proteasome inhibitors · Tumor angiogenesis · Tumor stroma · Tumor microenvironment

Introduction

Pancreatic ductal adenocarcinoma (PDAC) is a highly fatal malignancy with an overall 5-year survival rate of 10% in the USA [1]. Although the incidence of PDAC is rather low, comprising only 2.6% of worldwide cancer cases, it contributes to 4.7% of worldwide cancer-related deaths [2]. In the past decade, combination chemotherapies such as FOLFIRINOX and gemcitabine plus nab-paclitaxel have improved the survival of PDAC patients by several months [3, 4], but the overall response of PDAC to chemotherapies is very limited. The chemoresistance of PDAC may partly be attributed to its highly desmoplastic microenvironment, which can function as a barrier to effective drug delivery to PDAC cells [5]. The tumor microenvironment (TME) in PDAC, which is often referred as tumor stroma, is composed of pancreatic stellate cells (PSCs), extracellular matrix (ECM) proteins, tumor vasculature and immune cells. As the most abundant stromal cells and major ECM producers, PSCs are regarded as the key player in the desmoplastic reaction in PDAC [6]. The dynamic interaction among PSCs, cancer cells and other stroma components closely relates the progression and therapeutic escape of PDAC [7–10]. Moreover, studies have also shown that tumor stroma can restrain the progression of PDAC [11], highlighting the complex role of tumor stroma in pancreatic cancer. Recently, stroma-targeting approach has received great attention and emerged as a promising strategy to overcome chemoresistance in PDAC. Several agents have been proposed, yet none has been translated into clinical success [12].

✉ Wenhui Lou
lou.wenhui@zs-hospital.sh.cn

✉ Jianang Li
li.jian_ang@zs-hospital.sh.cn

[1] Department of Pancreatic Surgery, Zhongshan Hospital, Fudan University, 180 Fenglin Road, Shanghai 200032, China

MLN4924 is a first-in-class NEDD8-activating enzyme (NAE) inhibitor that has shown promising anti-tumor activities against hematological and solid malignancies [13]. MLN4924 acts primarily by inhibiting the Cullin-Ring ligases (CRLs), which are the largest family of E3 ubiquitin ligases. The activation of CRLs requires the binding of ubiquitin-like protein NEDD8 to the Cullin proteins, a modification known as neddylation, in which NEDD8 is activated by the NAE and conjugated to the Cullins via a three-step enzymatic cascade resembling the process of ubiquitination [14]. By binding to NEDD8 to form NEDD8-MLN4924 adducts in the presence of NAE, MLN4924 blocks the enzymatic activity of NAE, and ultimately inhibits the CRLs-mediated ubiquitin–proteasome system (UPS), which is responsible for the degradation of about 20% of cellular proteins [15]. Previous studies have shown that MLN4924 can suppress tumor cell growth by inducing DNA damage, apoptosis, senescence, apoptosis and autophagy [16–19], and of particular interest is that it can also inhibit angiogenesis during tumor development [20]. In our previous study, we found that MLN4924 inhibited the growth of PDAC cells directly [16], given the comprehensive effects that inhibiting UPS could have, we ask what impact MLN4924 would have on the stroma of pancreatic cancer. Here, we report that MLN4924 inhibited PSCs' growth and their secretion of collagen and CXCL-1, and the collagen secretion inhibiting effect of MLN4924 was related with transcription factor Gli1. We found that MLN4924 inhibited multiple angiogenic phenotypes of HMEC-1 cells, which could be partially relieved by mTOR agonist, and the angiogenesis inhibition effect of MLN4924 was related with REDD1 in HMEC-1 cells.

Materials and Methods

Cell Lines and Antibodies

Human microvascular endothelial cell line HMEC-1 was purchased from ATCC and cultured in MCDB131 medium (10372019, Life Technologies, Shanghai, China) supplemented with 10 ng/mL Epidermal Growth Factor (PHG0314, Thermofisher, Shanghai, China), 1 μg/mL Hydrocortisone (H0396, Sigma, Shanghai, China), 10% fetal bovine serum (Gibco, Shanghai, China), in a humidified 37 °C and 5% CO2 incubator. Anti-Vimentin (ab8978), anti-α-SMA (ab5694) and anti-REDD1 (ab191871) were purchased from Abcam, Shanghai, China. Anti-Gli1 (2643) was purchased from Cell Signaling Technology, Shanghai, China. Anti-GAPDH (sc-32233) and anti-β-actin (sc-69879) were purchased from Santa Cruz, Shanghai, China. Fluorescent dye-conjugated secondary antibodies (A-21201, A-11008) were obtained from Thermo Fisher Scientific, Shanghai, China. Horseradish peroxidase-conjugated secondary antibodies against mouse (sc-2005) and rabbit (sc-2004) were obtained from Santa Cruz.

Isolation and Culture of Human Pancreatic Stromal Outgrowths

The human PSC lines were established from fresh surgical specimens of pancreatic cancer using the outgrowth method described previously [21]. Fresh pancreatic tissue blocks (100–150 mg) were obtained from surgical samples of patients with pancreatic cancer undergoing pancreatic surgery at Zhongshan Hospital, Fudan University. This experiment was approved by the Ethics committee. The tissue blocks were cut into ~ 1 mm^3 pieces and seeded in a six-well plate in the presence of 10% FBS in a 1:1 (vol/vol) mixture of DMEM with Ham's F12 medium. 24 h after seeding, culture medium was changed, and 48 h later, the small tissue blocks were transferred to new culture plates. The PSCs grew out from the tissue blocks 1–3 days later. The small tissue blocks were removed after 2–3 weeks. Cells were passaged 1:3 when they reached 80% of confluence. The isolated cells were confirmed to be PSCs by their spindle-shaped morphology, loss of lipid droplets (assessed using the Lipid Staining Kit from Sigma-Aldrich, #MAK194, Shanghai, China) and immunofluorescence staining for αSMA and vimentin. Cell populations between passage 3 and 6 were used.

MTT Cell Viability Test

The 3-(4,5-Dimethylthiazol-2-yl)-2,5-diphenyltetrazolium bromide (MTT) method was used to detect cell viability. Briefly, 2000 cells were seeded in a 96-well plate and treated with MLN4924 of varied concentrations for 48 h. Then cells were incubated in 20% MTT (Sigma-Aldrich, Shanghai, China) diluted in a normal culture medium for an additional 4 h, and the absorbance was measured at a wavelength of 490 nm.

BrdU Proliferation Assay

After treatment, cells were incubated with bromodeoxyuridine (BrdU) labeling reagent for 30 min at 37 °C, following the manufacturer's instructions (Roche Diagnostics). Briefly, BrdU was added to the culture medium to a final concentration of 100 μM. After fixation with FixDenat for 30 min at room temperature, cells were incubated with Anti-BrdU-POD working solution for 90 min at room temperature. After washing, the tetramethylbenzidine substrate was added and incubated in the dark for 15 min. Then stop solution was added and absorbance was read at the wavelength of 450 nm using a microplate reader (Tecan infinite M2009PR).

Cell Apoptosis Assay

For apoptosis, cells were labeled using the Annexin V-PE apoptosis detection kit following the manufacturer's instructions (88-8007, eBioscience, San Diego, CA). Briefly, cells were harvested with trypsin, washed twice with ice-cold PBS, and resuspended in 1 × binding buffer. Then, 10 μl of annexin V-APC was added into 200ul of cell suspensions. After incubation for 15 min, the population study of the target cohort was performed by a flow cytometer (Guava easyCyte HT, Millipore, Burlington, USA).

Quantification of ECM Components

PSCs of different groups were treated accordingly for 48 h, and then the cell supernatants of each group were collected. Enzyme-linked immunosorbent assay (ELISA) kits were applied to detect the protein levels of CXCL-1 (CSB-E09150h, Cusabio Technology LLC, Wuhan, China) and MCP-1 (CSB-E04655h, Cusabio Technology LLC, Wuhan, China) in the supernatants following the instructions of the manufacturer. The Sircol Collagen Assay (Biocolor Ltd., Carrickfergus, UK) was used to detect the collagens in the supernatants following the instructions of the manufacturer.

RNAi Using shRNA

shRNA interference was used to decrease target gene expression according to the methods described previously [22]. The GV115 lentiviral vectors were designed and constructed by GeneChem Co., Ltd. (Shanghai, China). The human REDD1 shRNA target sequence was GGGCAAAGAACT ACTGCGCCT. Transfected clones were validated by qPCR and western immunoblot analysis.

Western Blotting

Total protein was extracted, and the concentration was measured using BCA protein assay (P0010S, Beyotime, Shanghai, China). 20–30 μg protein was separated on an 8–10% gel and electrotransferred onto polyvinylidene difluoride membranes (IPVH00010, Millipore, Shanghai, China). Membranes were incubated with antibodies as indicated in each figure. Then, the membranes were probed with HRP-conjugated secondary antibody for 1 h at room temperature. The protein bands were detected with ECL-PLUS reagent (32132, Thermo Fisher Scientific, Shanghai, China).

Immunofluorescence

Cells were seeded on coverslips and fixed with 4% paraformaldehyde for 10 min, then permeabilized with 0.2% Triton X-100 for 5 min at room temperature. Bovine serum albumin (BSA) was then used to block for 30 min at 37 °C. Cells were then incubated with primary antibody overnight at 4 °C, followed by incubation with Alexa Fluor 488-conjugated secondary antibodies at 37 °C for 45 min. Nuclei were stained for 5 min using DAPI. Subsequently, sections were sealed with antifade mounting medium and examined under a fluorescence microscope (Olympus IX71, Tokyo, Japan).

Quantitative Real-Time PCR

Total RNA was isolated using the Trizol reagent (Invitrogen, Carlsbad, CA, USA). Standard cDNA synthesis reactions were performed using the M-MLV Reverse Transcriptase kit (Promega, Shanghai, China) following the manufacturer's instructions. Reverse transcribed products were amplified using SYBR Premix Ex Taq (TaKaRa, Shanghai, China). PCR reactions were carried out using the LightCycler® 480 II Real-Time PCR system (Roche, USA) and repeated three times. Relative mRNA levels were normalized to GAPDH, and the relative expression of transcripts was analyzed using the $2^{-\Delta\Delta Ct}$ method. The following primers were used: human Gli1 (gene accession no. NM_005269): 5′- TTCCTA CCAGAGTCCCAAGT -3′ (forward) and 5′-CCCTATGTG AAGCCCTATTT -3′ (reverse); human REDD1 (gene accession no. NM_019058): 5′- TGACTTCAACAGCGACAC CCA -3′ (forward) and 5′-CACCCTGTTGCTGTAGCC AAA -3′ (reverse); human GAPDH: 5′-TGACTTCAACAG CGACACCCA-3′ (forward) and 5′-CACCCTGTTGCT GTA GCCAAA-3′ (reverse).

Cell Migration Assay

For cell migration assay, the transwell chamber (3422; Corning, Shanghai, China) was inserted into a 24-well culture plate. 1 × 105 cells suspended in 100 μl Dulbecco's modified Eagle's medium (DMEM) with or without MLN4924 were seeded in the upper chamber, and 600 μL of DMEM medium containing 30% FBS was added to the lower chamber. The transwell chamber was incubated for 48 h. The cells on the bottom surface of the filter were fixed in 4% paraformaldehyde and stained with Giemsa. Stained cells were counted in 9 randomly selected fields at ×200 magnification.

Capillary-Like Tube Formation Assay

We coated 96-well culture plates with Matrigel (70 μL/well) at 4 °C and incubated them for 30 min at 37 °C. HMEC-1 cells were seeded on the surface of the Matrigel and treated with MLN4924 and 3BDO for 24 h. After changing the medium, cells were dyed using 0.2 μM Calcein-AM (70 μL/well) for 5–10 min at 37 °C. Capillary tube formation was scanned with a confocal quantitative image cytometer (CQ1, Yokogawa Electric Corporation, Kanazawa, Japan). Images

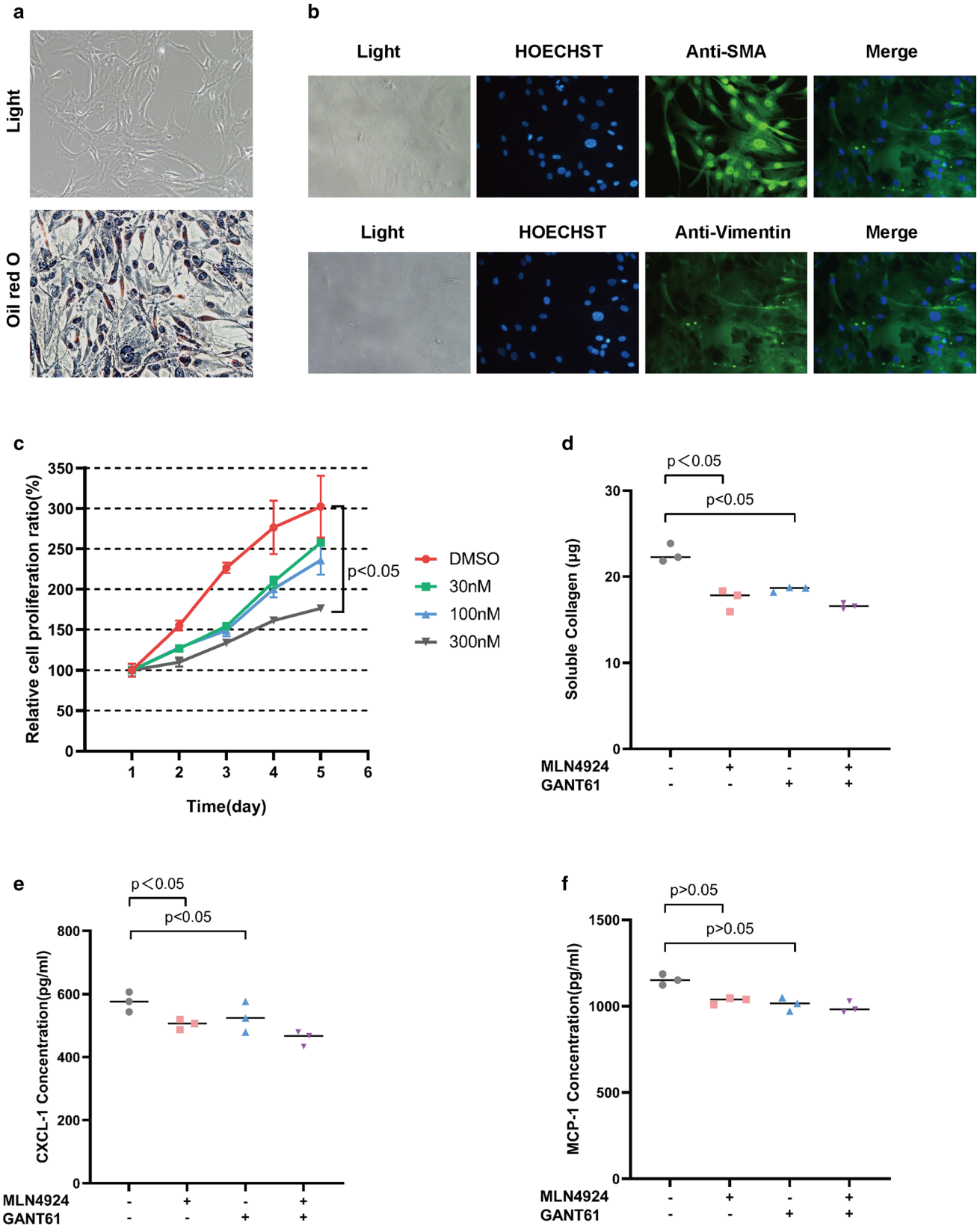
a
Light
Oil red O
b
Light
HOECHST
Anti-SMA
Merge
Light
HOECHST
Anti-Vimentin
Merge
c
Relative cell proliferation ratio(%)
Time(day)
DMSO
30nM
100nM
300nM
p<0.05
d
Soluble Collagen (μg)
p<0.05
p<0.05
MLN4924
GANT61
e
CXCL-1 Concentration(pg/ml)
p<0.05
p<0.05
MLN4924
GANT61
f
MCP-1 Concentration(pg/ml)
p>0.05
p>0.05
MLN4924
GANT61

◂**Fig. 1** MLN4924 inhibited PSCs' growth and the secretion of collagen and CXCL-1 **a** Representative microphotographs of activated human PSCs. PSCs were stellate-like or spindle-shaped in light microscopy, and lack of lipid droplets in the Oil Red O staining (original magnification: ×200). **b** Representative microphotographs of immunofluorescence staining of α-SMA and vimentin in PSCs. Activated human PSCs were confirmed by the positive staining of α-SMA and vimentin (original magnification: ×200). **c** MTT assay showed that MLN4924 inhibited the growth of PSCs in a dose-dependent manner. **d**–**e** The effects of MLN4924 and/or GANT61 on the secretion of collagen, CXCL-1 and MCP-1 of PSCs. PSCs were treated with MLN4924 (300 nM) and/or GANT61 (10 μM) for 48 h, then the concentration of soluble collagen in the supernatant of PSCs was measured using the Sircol Collagen Assay, and the concentrations of CXCL-1 and MCP-1 were measured using ELISA

were acquired with CQ1 (4× objective, 561 nm laser). Maximum intensity projection (MIP) images were constructed from 12 z slices (764 μm from bottom to top), then whole-well images were reconstructed from four adjacent images. The images were analyzed in the CQ1 software, and the length of line objects (μm), the number of branching points and the number of branches were counted.

Statistical Analysis

SPSS 24.0 (Chicago, IL, USA) was used for statistical analysis. Data from individual experiments were averaged and presented as the mean ± SD. The Student's t-test and ANOVA were used to compare quantitative variables. Significance was determined at $P < 0.05$.

Results

MLN4924 Inhibited PSCs' Growth and the Secretion of Collagen and CXCL-1

Activated human PSCs were confirmed by the positive staining of α-SMA, vimentin and loss of lipid droplets (Fig. 1a, b). MTT assay revealed that MLN4924 inhibited the proliferation of PSCs in a dose-dependent manner (Fig. 1c). Based on this result and previous reports that 300 nM of MLN4924 was sufficient to block neddylation and cause DNA damage [16, 23], we used 300 nM of MLN4924 for further experiments. We found that when treated with MLN4924, the concentration of collagen and CXCL-1 were decreased (Fig. 1d–f). It is well known that Sonic Hedgehog (Shh) pathway promotes desmoplasia in pancreatic cancer [24], so we tested if MLN4924 influenced the Shh pathway. When PSCs were treated with Shh inhibitor GANT61, we found that the concentrations of collagen and CXCL-1 were decreased (Fig. 1d–f). When PSCs were treated with MLN4924 combined with GANT61, the changing trends of the concentrations of collagen, CXCL-1 and MCP-1 were similar to these as treated with MLN4924 alone (Fig. 1d–f).

Collagen and CXCL-1 Secretion Inhibition of MLN4924 was Related with Transcription Factor Gli1

The secreted Shh binds to the Patched1 receptor and relieves repression of the 12-transmembrane protein Smoothened (Smo), resulting in activation of the Gli family of transcription factors. Since Gli1 could be degraded via CRLs-mediated UPS [25], we guessed that MLN4924 might act through upregulating Gli1 and thus activating Shh pathway. But contrary to our hypothesis, both the transcription and expression of Gli1 were decreased in PSCs when treated with MLN4924 (Fig. 2a). When Gli1 was effectively overexpressed (Fig. 2b), we observed that the proliferation of PSCs was increased slightly (Fig. 2c), and the secretions of collagen, CXCL-1 and MCP-1 were all promoted (Fig. 2d–f). Then we treated Gli1 overexpressed cells with MLN4924 and found that the proliferation of PSCs was partially inhibited (Fig. 2c). The secretions of collagen and CXCL-1 of Gli1 overexpressed cells treated with MLN4924 were decreased to the same level as that of control cells treated with MLN4924 or untreated Gli1 overexpression cells (Fig. 2d), suggesting that MLN4924 acts through Gli1 to inhibit collagen and CXCL-1 secretion of PSCs.

MLN4924 Inhibited Multiple Angiogenic Phenotypes of HMEC-1 Cells

Next, we used HMEC-1 cells, the first immortalized human microvascular endothelial cell line that retains the morphologic, phenotypic, and functional characteristics of normal human microvascular endothelial cells, to investigate how MLN4924 affects angiogenesis. The angiogenesis is assessed by measuring the area, skeleton length, junction count, and branch count of the vascular network-like structure formed by HMEC-1 cells (Fig. 3a). We can see that MLN4924 inhibited the angiogenesis in a dose-dependent manner (Fig. 3a–e). At the concentration of 300 nm of MLN4924, the area, skeleton length, junction count, and branch count of the vascular network-like structure were all significantly decreased (Fig. 3b–e). At the concentration of 300 nm, MLN4924 inhibited the viability and proliferation of HMEC-1 cells significantly, as manifested in the MTT assay and BrdU assay (Fig. 4a–b). MLN4924 also induced apoptosis in HMEC-1 cells (Fig. 4c) and inhibited the migration of HMEC-1 cells (Fig. 4d).

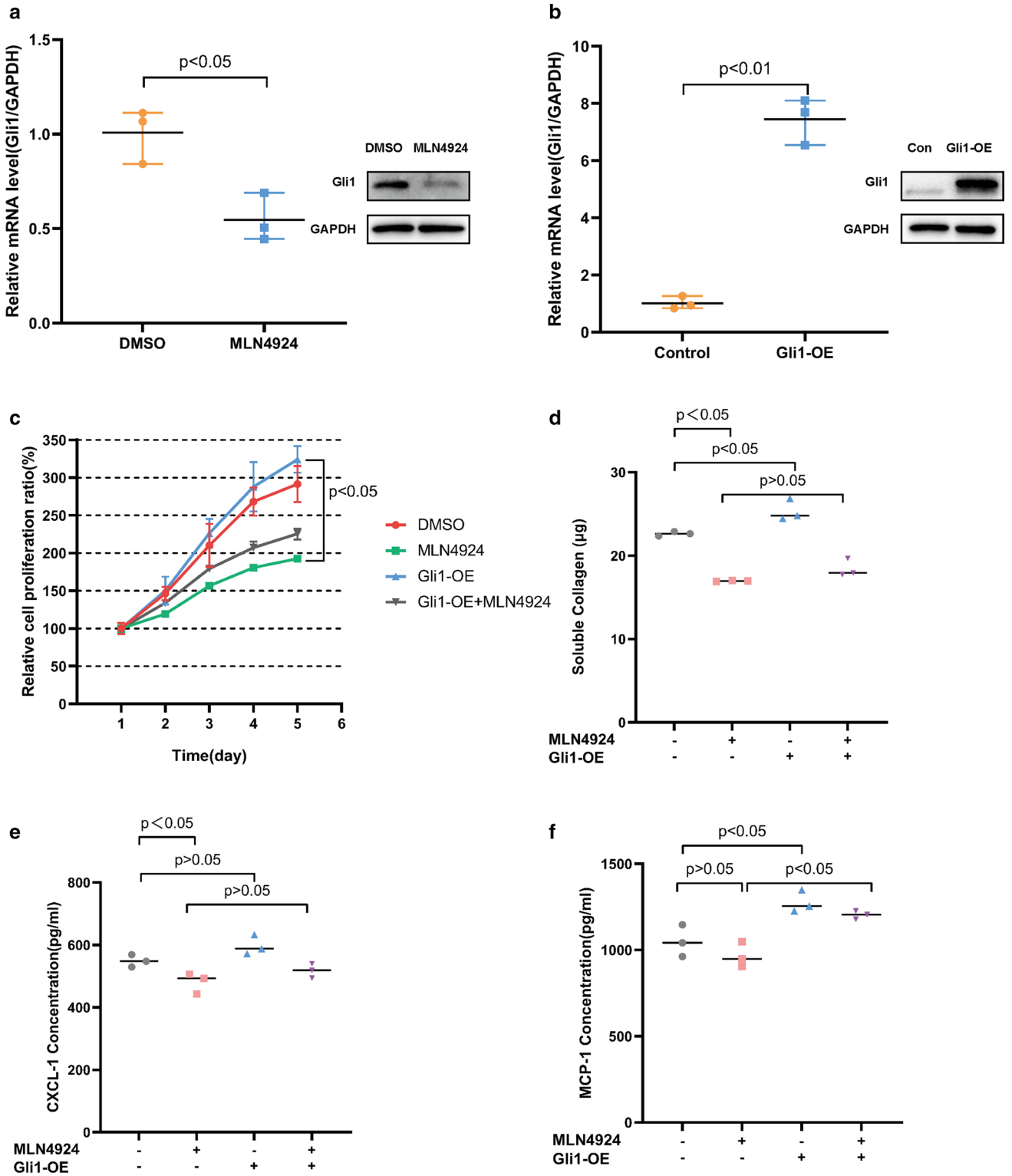

Fig. 2 The transcription factor Gli1 was decreased and was related with the collagen and CXCL-1 secretion inhibition of MLN4924 **a** RT-qPCR (left) and western blot (right) showed that the transcription and expression levels of Gli1 in PSCs were both inhibited after 48 h treatment of MLN4924. **b** RT-qPCR (left) and western blot (right) confirmed the effective overexpression of Gli1 in PSCs. **c** MTT assay showed that there were significant difference between the growth of Gli1 overexpressed cells and cells treated with MLN4924 ($P < 0.05$). **d–e** The effects of MLN4924 on the secretion of collagen, CXCL-1 and MCP-1 of control PSCs and Gli1 overexpressed PSCs. PSCs were treated with MLN4924 (300 nM) for 48 h, then the concentration of soluble collagen in the supernatant of PSCs was measured using the Sircol Collagen Assay, and the concentrations of CXCL-1 and MCP-1 were measured using ELISA

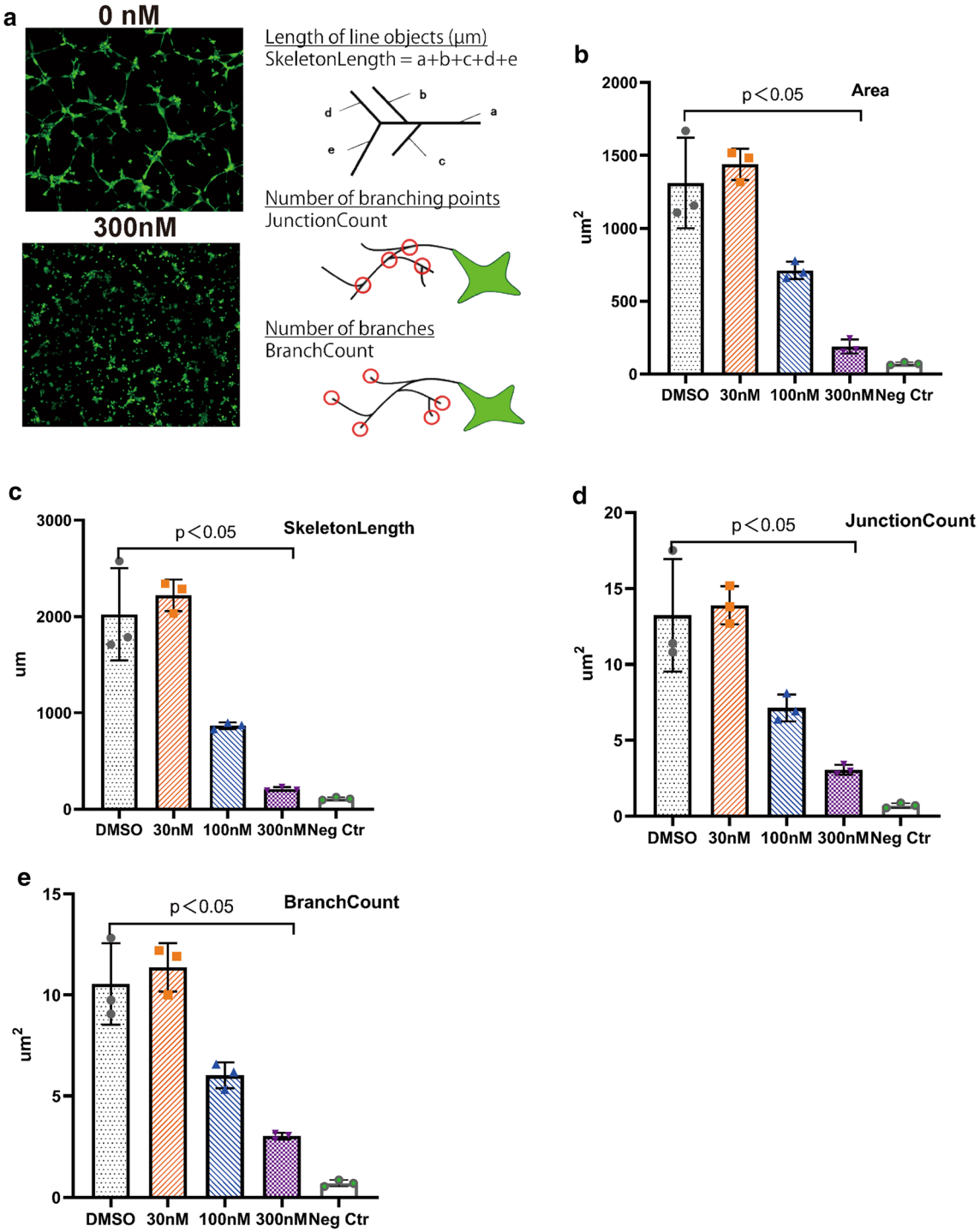

Fig. 3 MLN4924 inhibited the angiogenesis of HMEC-1 cells in a dose-dependent manner. After cells were treated with MLN4924 at indicated concentrations for 48 h, Capillary-like tube formation assay was performed. **a** Representative microphotographs of the vascular network-like structure formed by HMEC-1 cells (original magnification: × 10). **b–e** The area, skeleton length, number of branching points and number of branches of the vascular network-like structure formed by HMEC-1 cells after MLN4924 treatment

REDD1 Knockdown Reversed the Inhibition of MLN4924 on HEMC-1 Cells

As PDAC is characterized by a desmoplastic reaction that creates a hypoxia microenvironment [26, 27], which leads to mTOR inhibition, so we tested the effects of mTOR agonist 3BDO combined with MLN4924 on HMEC-1 cells. 3BDO did not affect cell viability (Fig. 4a), but partly relieved the capillary tube formation inhibition of HMEC-1 cells (Fig. 5a–e). And because REDD1 (regulated

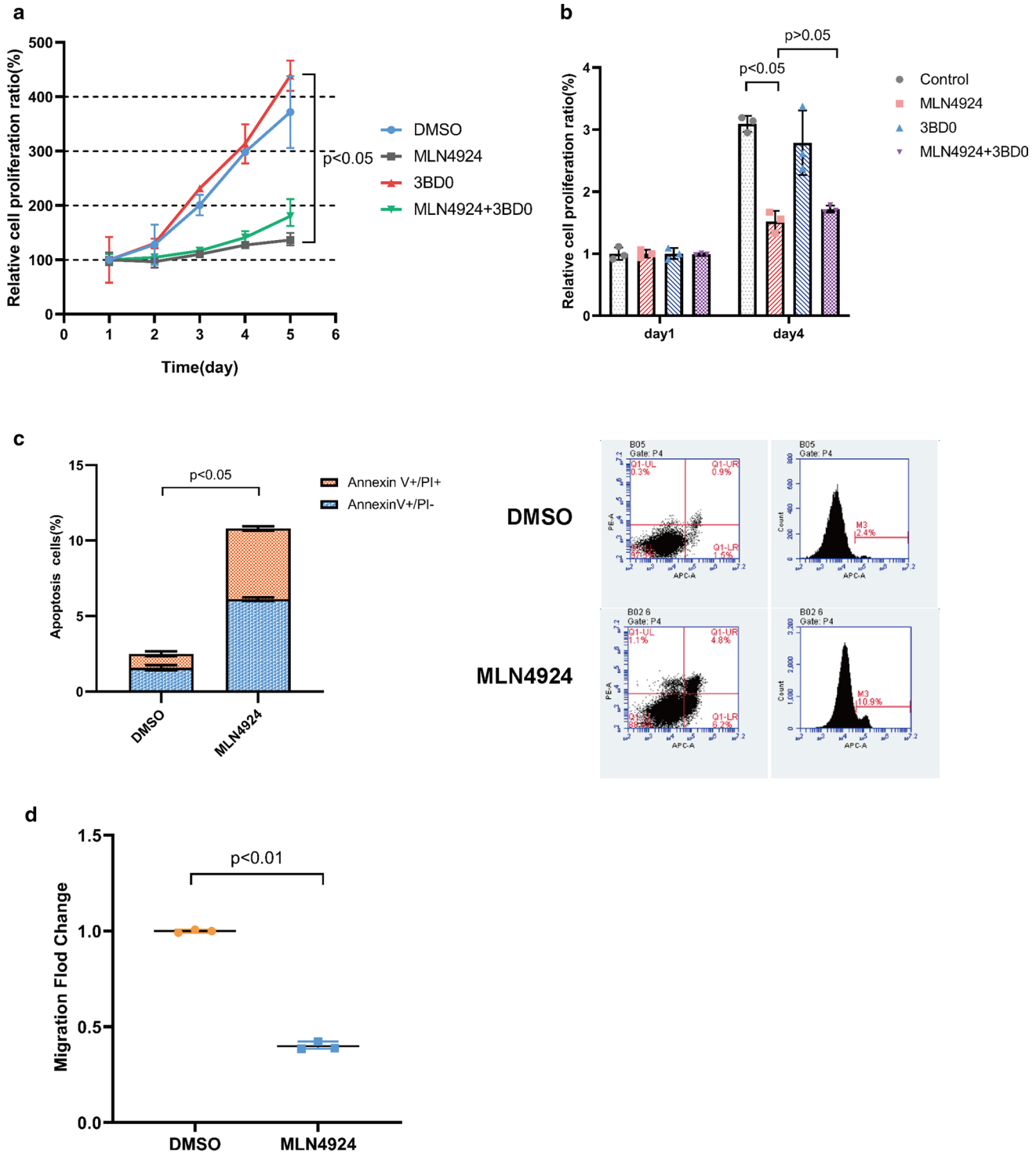

Fig. 4 MLN4924 inhibited the growth and migration of HMEC-1 cells and induced apoptosis in HMEC-1 cells **a** MTT assay showed that MLN4924 inhibited the growth of HMEC-1 cells significantly. **b** BrdU assay showed that MLN4924 inhibited the proliferation of HMEC-1 cells significantly. **c** FACS analysis showed that the percentage of apoptotic cells (Annexin V + and PI ±) was increased in HMEC-1 cells treated with MLN4924. **d** Migration assay showed that MLN4924 inhibited the migration of HMEC-1 cells significantly

in development and DNA damage responses 1) is a CRLs substrate and is known to have a crucial role in inhibiting mTOR signaling during hypoxic stress [28, 29], we suspect that REDD1 would be regulated by MLN4924. We evaluated the impact of MLN4924 on REDD1 expression, and found that MLN4924 promoted the transcription and expression of

REDD1 (Fig. 5a). When REDD1 was effectively knocked down using RNAi (Fig. 5b), the capillary tube formation of HMEC-1 cells was significantly promoted and could reverse the effect of MLN4924 (Fig. 5c–g).

Discussion

Ever since the discovery of MLN4924 in 2009, much research has been conducted regarding its anti-tumor activities and underlying mechanisms against various kinds of neoplasms, including pancreatic cancer. As abundant desmoplastic stroma is a hallmark of PDAC and is considered an important participant of disease progression, what effect MLN4924 would have on pancreatic cancer stroma is a question worth investigating. There have been reports that MLN4924 inhibits tumor vasculature [20, 30], but no studies regarding its specific mechanisms and the effect of MLN4924 on other components of tumor stroma have been published. Here we evaluated the impact of MLN4924 on PSCs established from fresh surgical specimens of pancreatic cancer and HMEC-1 cells in vitro and explored possible underlying mechanisms.

We found that although MLN4924 inhibited the growth and the secretion of collagen and CXCL-1 of PSCs. The rationale of stroma-targeting therapy has been that the dense stroma hinders the delivery of chemotherapy drugs [31], enhance cancer cell proliferation and invasion [32, 33], and also contributes to immune suppression [34]. However, as clinical trials assessing stroma-targeting therapies yielded disappointing results, the anti-tumor potential of the PDAC stroma has also been gradually revealed. Part of the reasons for these disappointing results are that most of pancreatic cancer live in hypoxic tumor microenvironment, therefore anti-angiogenic agents directed against the ligand may have limited effects. And In preclinical models, reducing the PDAC stroma leads to more invasive and undifferentiated tumors, with diminished animal survival [11, 35]. Furthermore, different subtypes of cancer-associated fibroblasts (CAF) have different effects on anti-tumor drugs. The targeted inhibition of IL6, presumably produced by the inflammatory CAF population, was shown to enhance the efficacy of anti–PD-L1 in PDAC. However, the aSMA-positive CAF population is regulated by Hedgehog signaling but has a tumor-suppressive function [36, 37]. Since increased levels of Shh (Sonic hedgehog) expression are observed throughout PDAC tumorigenesis and thought to play an important role in PDAC desmoplasia [38], we explored whether MLN4924 acted via the Shh pathway. Indeed, we found that the effects of Gli1 inhibitor GANT61 were similar to MLN4924. And Gli1, the robust activator that mediate the transcriptional effects of the Shh pathway, was decreased in PSCs when treated with MLN4924. Although Gli1 is regulated by CRLs-mediated degradation [39], the experimental results are contrary to our original hypothesis that Gli1 is elevated after MLN4924 treatment, and it is speculated that other regulation mechanisms might be involved in the reduction of Gli1, and some further researches are need. It is reported that Shh overexpression or Gli1 protein accumulation promotes tumor growth and contributes to the invasiveness of pancreatic cancer [25, 40], but Simon et al. [41] also reported that Gli1 inhibition promotes epithelial-to-mesenchymal transition in pancreatic cancer cells, so the overall effects of Gli1 inhibition in PDAC by MLN4924 should be evaluated more comprehensively.

Chemokines have a broad range of effects on the recruitment and function of inflammatory cells. Chemokines in malignancy are generally considered as having tumor-promoting roles, although there are cases in which chemokines are implicated as having tumor-inhibiting activities [42]. CXCL-1 is involved in carcinogenesis of melanoma and promotes the invasion and metastasis of gastric cancer, breast cancer and colorectal cancer [43–46]. MCP-1, a CC chemokine able to attract macrophages, was reported to be a relevant negative regulator of pancreatic cancer progression [47]. The recruited monocytes manifested a direct antiproliferative and proapoptotic activity toward pancreatic cancer cell in vitro. However, there are reports that MCP-1 promotes the invasion of prostate cancer, ovarian cancer, and breast cancer [48–50]. Generally, the functions of chemokines may be different depending on the tumor type and chemokine type. The biological significance of CXCL-1 secretion inhibition by MLN4924 awaits further elucidation. There are few studies regarding the regulation of CXCL-1 and MCP-1 secretion, our study suggests that CRLs-mediated UPS may be involved, and related with the transcription factor Gli1.

REDD1, a known CRLs substrate, was increased when treated with MLN4924. Our results are similar to the study of Gu et al. [51], which shows that MLN4924 induces REDD1 expression in human myeloma cells. Previous studies have found that MLN4924 simultaneously improves the transcription level and protein stability of REDD1 [51]. It is reasonable to assume that other regulating mechanisms other than CRLs-mediated degradation is involved in the reduction of REDD1. Presently REDD1 is mainly considered a stress-response gene that is regulated by hypoxia via hypoxia-inducible factor 1 (HIF-1) and by DNA damage via p53/p63 [52], it might also be regulated by STAT3 on mRNA level [53]. Our following knockdown experiments further support an important role for REDD1 in the maintaining of angiogenic phenotypes of HMEC-1 cells, but further research is needed to fully elucidate the functions and regulatory mechanisms of REDD1. Previous studies reported that neddylation inhibition leads to tumor angiogenesis suppression and hypoxia partly reverses the angiogenesis suppression

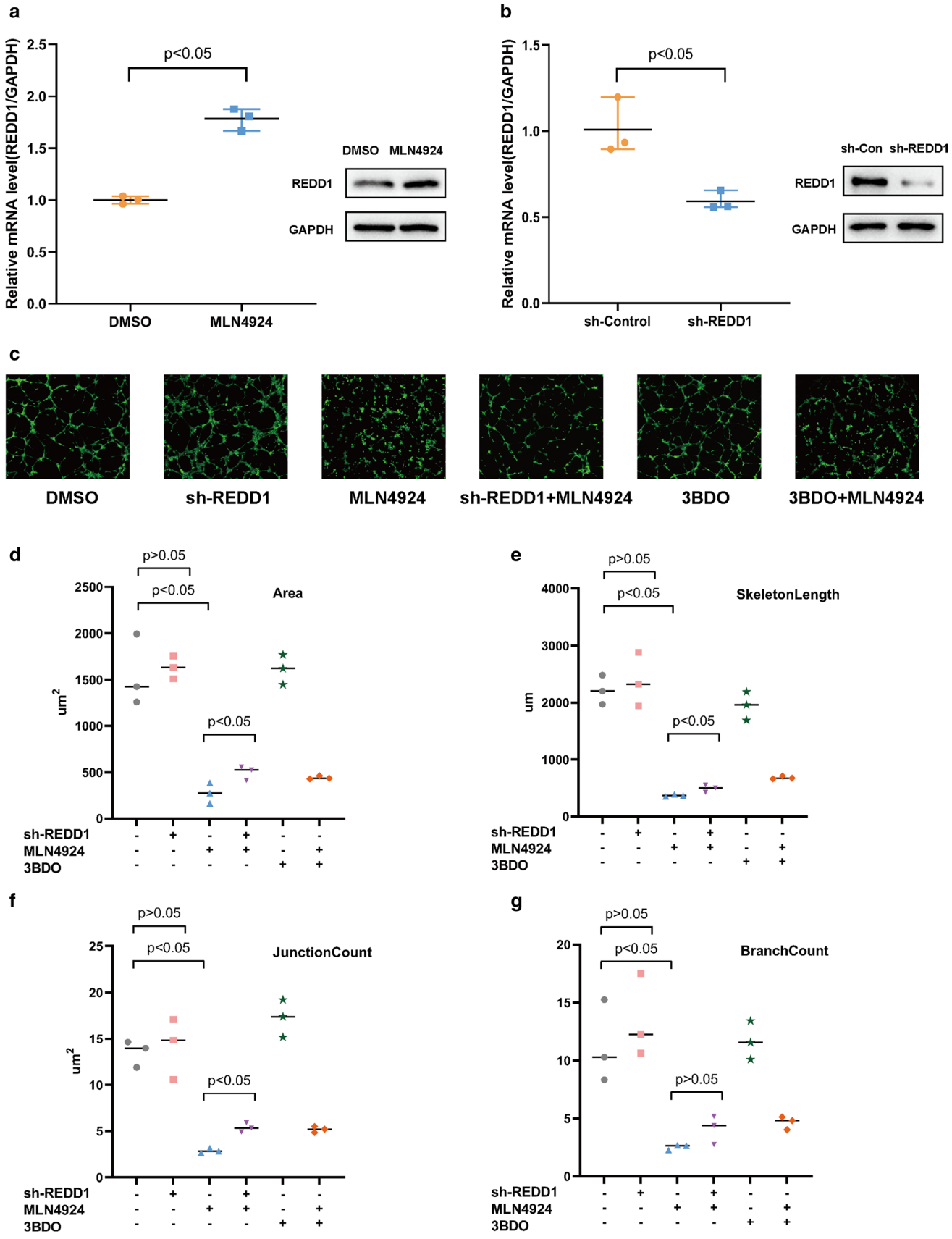
a
Relative mRNA level(REDD1/GAPDH)
p<0.05
DMSO
MLN4924
DMSO MLN4924
REDD1
GAPDH
b
Relative mRNA level(REDD1/GAPDH)
p<0.05
sh-Control
sh-REDD1
sh-Con sh-REDD1
REDD1
GAPDH
c
DMSO
sh-REDD1
MLN4924
sh-REDD1+MLN4924
3BDO
3BDO+MLN4924
d
Area
um2
p>0.05
p<0.05
p<0.05
sh-REDD1
MLN4924
3BDO
e
SkeletonLength
um
p>0.05
p<0.05
p<0.05
sh-REDD1
MLN4924
3BDO
f
JunctionCount
um2
p>0.05
p<0.05
p<0.05
sh-REDD1
MLN4924
3BDO
g
BranchCount
p>0.05
p<0.05
p>0.05
sh-REDD1
MLN4924
3BDO

◂**Fig. 5** REDD1 was increased by MLN4924 and REDD1 knockdown promoted the angiogenesis of HMEC-1 cells The mTOR agonist 3BDO partially relieved the inhibition of MLN4924 on HEMC-1 cells. **a** RT-qPCR (left) and western blot (right) showed that the transcription and expression levels of REDD1 in HMEC-1 cells were both promoted after 48 h treatment of MLN4924. **b** RT-qPCR (left) and western blot (right) confirmed the effective knockdown of REDD1 in HMEC-1 cells. **c** Representative microphotographs of the vascular network-like structure formed by HMEC-1 cells (original magnification: × 10). **d**–**g** Cells were treated with MLN4924 and/or 3BDO (20 μM) for 48 h, and capillary-like tube formation assay was performed. The area, skeleton length, number of branching points and number of branches of the vascular network-like structure formed by HMEC-1 cells treated as indicated

[20, 30], but the exact mechanism has not been revealed. As mTOR is activated in response to hypoxia [54], meanwhile MLN4924 inhibits mTOR signaling transduction [55], we hypothesized that mTOR signaling might be involved in this process. Indeed, we found that mTOR agonist 3BDO partly relieved the inhibition effects of MLN4924.

There are several limitations of our study. Firstly, we did not take into account the heterogeneity of PSCs. Recently there have been many studies on the functional heterogeneity of PSC subpopulations with different biomarkers [32, 56–59], it is possible that different subsets of PSCs may react differently to MLN4924. Secondly, although our results revealed the possible molecular mechanisms of the stroma-remodeling effect of MLN4924, but it still needs further investigation and validation. Thirdly, we didn't perform in vivo experiments due to our limited resources. Further animal experiments using models that mimic the tumor stroma of human PDAC, such as KPC mouse model [60], will help to clarify the stroma-remodeling effects of MLN4924.

In summary, our data are significant in that they demonstrate the comprehensive stroma-remodeling effects of MLN4924 and reveal possible underlying mechanisms. We find MLN4924 inhibits the PSCs and their secretion of collagen, which could be partially mediated by Gli1, but the therapeutic effect of stroma-depleting therapy is still debating. MLN4924 also exhibits anti-angiogenesis effects that are related with an increased expression of REDD1. Our study increases the understanding of the multi-facets of the effect of MLN4924 and supports further translational studies.

Acknowledgments This work was supported by the National Natural Science Foundation of China [Grant Numbers 81903066, 81773068].

Author's Contribution All authors contributed to the study conception and design. Material preparation, data collection and analysis were performed by Weilin Mao, Lei Zhang and Yefei Rong. The first draft of the manuscript was written by Jianang Li and Weilin Mao, and all authors commented on previous versions of the manuscript. All authors read and approved the final manuscript.

Funding This work was supported by the National Natural Science Foundation of China [Grant Numbers 81903066, 81773068].

Data Availability The datasets generated and analyzed during the current study are available from the corresponding author on reasonable request.

Declarations

Conflict of interest The authors declare that they have no conflicts of interest.

References

1. Mizrahi JD, Surana R, Valle JW, Shroff RT. Pancreatic cancer. *The Lancet* 2020;395:2008–2020. https://doi.org/10.1016/S0140-6736(20)30974-0.
2. Sung H, Ferlay J, Siegel RL et al. Global cancer statistics 2020: GLOBOCAN estimates of incidence and mortality worldwide for 36 cancers in 185 countries. *CA Cancer J Clin* 2021;71:209–249.
3. Conroy T, Desseigne F, Ychou M et al. FOLFIRINOX versus Gemcitabine for Metastatic Pancreatic Cancer. *N Engl J Med* 2011;364:1817–1825. https://doi.org/10.1056/NEJMoa1011923.
4. Von Hoff DD, Ervin T, Arena FP et al. Increased Survival in Pancreatic Cancer with nab-Paclitaxel plus Gemcitabine. *N Engl J Med* 2013;369:1691–1703. https://doi.org/10.1056/NEJMoa1304369.
5. Amrutkar M, Gladhaug IP. Pancreatic cancer chemoresistance to gemcitabine. *Cancers* 2017;9:157.
6. Apte M, Park S, Phillips P et al. Desmoplastic reaction in pancreatic cancer: role of pancreatic stellate cells. *Pancreas* 2004;29:179–187.
7. Biffi G, Oni TE, Spielman B et al. IL1-induced JAK/STAT signaling is antagonized by TGFβ to shape CAF heterogeneity in pancreatic ductal adenocarcinoma. *Cancer Discov* 2019;9:282–301.
8. Hessmann E, Patzak M, Klein L et al. Fibroblast drug scavenging increases intratumoural gemcitabine accumulation in murine pancreas cancer. *Gut* 2018;67:497–507.
9. Yoshida N, Masamune A, Hamada S et al. Kindlin-2 in pancreatic stellate cells promotes the progression of pancreatic cancer. *Cancer Lett* 2017;390:103–114.
10. Qian D, Lu Z, Xu Q et al. Galectin-1-driven upregulation of SDF-1 in pancreatic stellate cells promotes pancreatic cancer metastasis. *Cancer Lett* 2017;397:43–51.
11. Rhim AD, Oberstein PE, Thomas DH et al. Stromal elements act to restrain, rather than support, pancreatic ductal adenocarcinoma. *Cancer Cell* 2014;25:735–747.
12. Vennin C, Murphy KJ, Morton JP, Cox TR, Pajic M, Timpson P. Reshaping the tumor stroma for treatment of pancreatic cancer. *Gastroenterology* 2018;154:820–838.
13. Park J, Cho J, Song EJ. Ubiquitin–proteasome system (UPS) as a target for anticancer treatment. *Arch Pharm Res* 2020:1–18.
14. Zhao Y, Morgan MA, Sun Y. Targeting Neddylation pathways to inactivate cullin-RING ligases for anticancer therapy. *Antioxid Redox Signal* 2014;21:2383–2400.
15. Lan H, Tang Z, Jin H, Sun Y. Neddylation inhibitor MLN4924 suppresses growth and migration of human gastric cancer cells. *Sci Rep* 2016;6:24218. https://doi.org/10.1038/srep24218.
16. Li J, Song C, Rong Y et al. Chk1 inhibitor SCH 900776 enhances the antitumor activity of MLN4924 on pancreatic cancer. *Cell Cycle* 2018;17:191–199.
17. Luo Z, Yu G, Lee HW et al. The Nedd8-activating enzyme inhibitor MLN4924 induces autophagy and apoptosis to suppress liver cancer cell growth. *Cancer Res* 2012;72:3360–3371.

18. Lin JJ, Milhollen MA, Smith PG, Narayanan U, Dutta A. NEDD8-targeting drug MLN4924 elicits DNA rereplication by stabilizing Cdt1 in S phase, triggering checkpoint activation, apoptosis, and senescence in cancer cells. *Cancer Res* 2010;70:10310–10320.
19. Lin S, Shang Z, Li S et al. Neddylation inhibitor MLN4924 induces G2 cell cycle arrest, DNA damage and sensitizes esophageal squamous cell carcinoma cells to cisplatin. *Oncol Lett* 2018;15:2583–2589.
20. Yao W, Wu J, Yu G et al. Suppression of tumor angiogenesis by targeting the protein neddylation pathway. *Cell Death Dis* 2014;5:e1059–e1059.
21. Bachem MG, Schünemann M, Ramadani M et al. Pancreatic carcinoma cells induce fibrosis by stimulating proliferation and matrix synthesis of stellate cells. *Gastroenterology* 2005;128:907–921.
22. Fang Y, Han X, Li J, Kuang T, Lou W. HEATR1 deficiency promotes chemoresistance via upregulating ZNF185 and downregulating SMAD4 in pancreatic cancer. *J Oncol* 2020;2020.
23. Soucy TA, Smith PG, Milhollen MA et al. An inhibitor of NEDD8-activating enzyme as a new approach to treat cancer. *Nature* 2009;458:732–736. https://doi.org/10.1038/nature07884.
24. Bailey JM, Swanson BJ, Hamada T et al. Sonic hedgehog promotes desmoplasia in pancreatic cancer. *Clin Cancer Res* 2008;14:5995–6004.
25. Huntzicker EG, Estay IS, Zhen H, Lokteva LA, Jackson PK, Oro AE. Dual degradation signals control Gli protein stability and tumor formation. *Genes Dev* 2006;20:276–281.
26. Erkan M, Kurtoglu M, Kleeff J. The role of hypoxia in pancreatic cancer: a potential therapeutic target? *Expert Rev Gastroenterol Hepatol* 2016;10:301–316.
27. Humar R, Kiefer FN, Berns H, Resink TJ, Battegay EJ. Hypoxia enhances vascular cell proliferation and angiogenesis in vitro via rapamycin (mTOR)-dependent signaling. *FASEB J* 2002;16:771–780.
28. Katiyar S, Liu E, Knutzen CA et al. REDD1, an inhibitor of mTOR signalling, is regulated by the CUL4A–DDB1 ubiquitin ligase. *EMBO Rep* 2009;10:866–872.
29. Brugarolas J, Lei K, Hurley RL et al. Regulation of mTOR function in response to hypoxia by REDD1 and the TSC1/TSC2 tumor suppressor complex. *Genes Dev* 2004;18:2893–2904.
30. Shi C-S, Kuo K-L, Lin W-C et al. Neddylation inhibitor, MLN4924 suppresses angiogenesis in huvecs and solid cancers: in vitro and in vivo study. *Am J Cancer Res* 2020;10:953.
31. Olive KP, Jacobetz MA, Davidson CJ et al. Inhibition of Hedgehog signaling enhances delivery of chemotherapy in a mouse model of pancreatic cancer. *Science* 2009;324:1457–1461.
32. Ikenaga N, Ohuchida K, Mizumoto K et al. CD10+ pancreatic stellate cells enhance the progression of pancreatic cancer. *Gastroenterology* 2010;139:1041–1051.
33. Lonardo E, Frias-Aldeguer J, Hermann PC, Heeschen C. Pancreatic stellate cells form a niche for cancer stem cells and promote their self-renewal and invasiveness. *Cell Cycle* 2012;11:1282–1290.
34. Thind K, Padrnos LJ, Ramanathan RK, Borad MJ. Immunotherapy in pancreatic cancer treatment: a new frontier. *Ther Adv Gastroenterol* 2017;10:168–194.
35. Özdemir BC, Pentcheva-Hoang T, Carstens JL et al. Depletion of carcinoma-associated fibroblasts and fibrosis induces immunosuppression and accelerates pancreas cancer with reduced survival. *Cancer Cell* 2014;25:719–734.
36. Huang H, Brekken RA. The Next Wave of Stroma-Targeting Therapy in Pancreatic Cancer. *Cancer Res* 2019;79:328–330.
37. van Mackelenbergh MG, Stroes, CI, Spijker R et al. Clinical Trials Targeting the Stroma in Pancreatic Cancer: A Systematic Review and Meta-Analysis. *Cancers (Basel)*, 2019. 11(5).
38. Thayer SP, di Magliano MP, Heiser PW et al. Hedgehog is an early and late mediator of pancreatic cancer tumorigenesis. *Nature* 2003;425:851–856.
39. Hui C, Angers S. Gli proteins in development and disease. *Annu Rev Cell Dev Biol* 2011;27:513–537.
40. Nagai S, Nakamura M, Yanai K et al. Gli1 contributes to the invasiveness of pancreatic cancer through matrix metalloproteinase-9 activation. *Cancer Sci* 2008;99:1377–1384.
41. Joost S, Almada LL, Rohnalter V et al. GLI1 inhibition promotes epithelial-to-mesenchymal transition in pancreatic cancer cells. *Cancer Res* 2012;72:88–99.
42. Mishra P, Banerjee D, Ben-Baruch A. Chemokines at the crossroads of tumor-fibroblast interactions that promote malignancy. *J Leukoc Biol* 2011;89:31–39.
43. Dhawan P, Richmond A. Role of CXCL1 in tumorigenesis of melanoma. *J Leukoc Biol* 2002;72:9–18.
44. Cheng W-L, Wang C-S, Huang Y-H, Tsai M-M, Liang Y, Lin K-H. Overexpression of CXCL1 and its receptor CXCR2 promote tumor invasion in gastric cancer. *Ann Oncol* 2011;22:2267–2276.
45. Wang N, Liu W, Zheng Y et al. CXCL1 derived from tumor-associated macrophages promotes breast cancer metastasis via activating NF-κB/SOX4 signaling. *Cell Death Dis* 2018;9:1–18.
46. Wang D, Sun H, Wei J, Cen B, DuBois RN. CXCL1 is critical for premetastatic niche formation and metastasis in colorectal cancer. *Cancer Res* 2017;77:3655–3665.
47. Monti P, Leone BE, Marchesi F et al. The CC chemokine MCP-1/CCL2 in pancreatic cancer progression: regulation of expression and potential mechanisms of antimalignant activity. *Cancer Res* 2003;63:7451–7461.
48. Lu Y, Chen Q, Corey E et al. Activation of MCP-1/CCR2 axis promotes prostate cancer growth in bone. *Clin Exp Metastasis* 2009;26:161–169.
49. Furukawa S, Soeda S, Kiko Y et al. MCP-1 promotes invasion and adhesion of human ovarian cancer cells. *Anticancer Res* 2013;33:4785–4790.
50. Dutta P, Sarkissyan M, Paico K, Wu Y, Vadgama JV. MCP-1 is overexpressed in triple-negative breast cancers and drives cancer invasiveness and metastasis. *Breast Cancer Res Treat* 2018;170:477–486.
51. Gu Y, Kaufman JL, Bernal L et al. MLN4924, an NAE inhibitor, suppresses AKT and mTOR signaling via upregulation of REDD1 in human myeloma cells. *Blood* 2014;123:3269–3276. https://doi.org/10.1182/blood-2013-08-521914.
52. Jin H-O, An S, Lee H-C et al. Hypoxic condition-and high cell density-induced expression of Redd1 is regulated by activation of hypoxia-inducible factor-1α and Sp1 through the phosphatidylinositol 3-kinase/Akt signaling pathway. *Cell Signal* 2007;19:1393–1403.
53. Pinno J, Bongartz H, Klepsch O et al. Interleukin-6 influences stress-signalling by reducing the expression of the mTOR-inhibitor REDD1 in a STAT3-dependent manner. *Cell Signal* 2016;28:907–916.
54. Li W, Petrimpol M, Molle KD, Hall MN, Battegay EJ, Humar R. Hypoxia-induced endothelial proliferation requires both mTORC1 and mTORC2. *Circ Res* 2007;100:79–87.
55. Guo N, Azadniv M, Coppage M et al. Effects of neddylation and mTOR inhibition in acute myelogenous leukemia. *Transl Oncol* 2019;12:602–613.
56. Öhlund D, Handly-Santana A, Biffi G et al. Distinct populations of inflammatory fibroblasts and myofibroblasts in pancreatic cancer. *J Exp Med* 2017;214:579–596.
57. Tjomsland V, Aasrum M, Christoffersen T, Gladhaug IP. Functional heterogeneity in tumor-derived human pancreatic stellate cells: Differential expression of HGF and implications for mitogenic signaling and migration in pancreatic cancer cells. *Oncotarget* 2017;8:71672.

58. Fujiwara K, Ohuchida K, Mizumoto K et al. CD271+ subpopulation of pancreatic stellate cells correlates with prognosis of pancreatic cancer and is regulated by interaction with cancer cells. *PloS One* 2012;7:e52682.
59. Farrow B, Rowley D, Dang T, Berger DH. Characterization of tumor-derived pancreatic stellate cells. *J Surg Res* 2009;157:96–102.
60. Hingorani SR, Wang L, Multani AS et al. Trp53R172H and KrasG12D cooperate to promote chromosomal instability and widely metastatic pancreatic ductal adenocarcinoma in mice. *Cancer Cell* 2005;7:469–483.